

Minimal nonabelian model of atomic dark matter

Jeremie Choquette^{*1} and James M. Cline^{†1,2}

¹*Department of Physics, McGill University, 3600 Rue University, Montréal, Québec, Canada H3A 2T8*

²*Niels Bohr International Academy and Discovery Center, Niels Bohr Institute,
University of Copenhagen, Blegdamsvej 17, DK-2100 Copenhagen Ø, Denmark*

A dark sector resembling the standard model, where the abundance of matter is explained by baryon and lepton asymmetries, and stable constituents bind to form atoms, is a theoretically appealing possibility. We show that a minimal model with a hidden $SU(2)$ gauge symmetry broken to $U(1)$, with a Dirac fermion doublet, suffices to realize this scenario. Supplemented with a dark Higgs doublet that gets no VEV, we readily achieve the dark matter asymmetry through leptogenesis. The model can simultaneously have three portals to the standard model, through the Higgs, nonabelian kinetic mixing, and the heavy neutrino, with interesting phenomenology for direct and collider searches, as well as cosmologically relevant DM self-interactions. Exotic bound states consisting of two fermions and a doubly-charged vector boson can exist in one phase of the theory.

Dark matter (DM) from a hidden sector has been a popular alternative to supersymmetric weakly interacting massive particles in recent years [1, 2]. A widely studied example is dark atoms, where the DM consists of two species with opposite charges under an unbroken $U(1)_h$ hidden sector gauge symmetry [3–9]. This class of models presents rich possibilities for direct detection [10–13], as well as cosmological imprints [14–19]. If the hidden photon has kinetic mixing with the normal photon, the dark constituents acquire electric millicharges [20], leading to further constraints and prospects for detection [21–23].

Simplified models of atomic dark matter are easy to construct, consisting of just two fermions and the gauge boson in the hidden sector, but such examples are necessarily incomplete descriptions of the new physics required. First, it is desirable for the DM to be asymmetric, otherwise the long-range $U(1)_h$ interaction would leave too small a relic abundance unless the DM mass exceeds ~ 400 GeV [24]¹. Simplified models do not explain the origin of the asymmetry. Second, the $U(1)_h$ gauge interaction leads to a Landau pole at high energies, so it would be desirable to find a more UV-complete version of the theory. Third, dark constituent millicharges greater than $\sim 10^{-7}e$ (of interest for collider searches) require the atomic constituents to be nearly equal in mass, which is a rather ad hoc requirement in the simplified models. In this work we present a model that is still relatively simple, but addresses both of these issues, and makes a number of interesting experimental predictions. It relies upon breaking a nonabelian (hence asymptotically free) gauge symmetry $SU(2)_h$ down to $U(1)_h$ to explain the origin of the massless dark photon. The approximate equality

of the dark constituents, if desired, can be explained as a remnant of the gauge symmetry.

There have been many proposals for mechanisms that link the asymmetries of the hidden and visible sectors. In general, they tend to be complicated. A notable exception is to use the out-of-equilibrium decays of heavy neutrinos to generate both asymmetries via leptogenesis and its analog in the hidden sector [5, 25–30]. We adopt this approach here.

The model presents opportunities for direct detection, either through Higgs portal interactions or nonabelian gauge kinetic mixing. The latter can arise through a dimension-5 operator involving the triplet Higgs field that breaks the $SU(2)_h$ gauge symmetry [31]. This results in electric millicharges for the dark matter constituents, that normally must be very small to avoid direct detection, but can be sizable if the dark constituents have equal mass, which is a symmetry limit of the theory presented here. Moreover the self-interactions of the dark atoms can be of the right magnitude for addressing problems of small-scale structure formation in standard noninteracting Λ CDM cosmology.

In the following we introduce the model (section 1) and then estimate the dark matter and baryon asymmetries that can arise in a generic scenario for leptogenesis (section 2). Limits from direct searches are worked out in section 3. In section 4 we consider the region of parameter space in which the vector bosons are stable, leading to a markedly different dark sector. In sect. 5 we discuss constraints pertaining to the ionization fraction, dark atom self-interactions, and searches for millicharged particles. Conclusions are given in sect. 6.

1. THE MODEL

The new-physics content of the model (summarized in table I) is a hidden $SU(2)_h$ gauge boson B_μ with field strength $B_{\mu\nu}^a$, a real scalar triplet ϕ that spontaneously breaks $SU(2)_h$ by getting a VEV, a scalar doublet η that does not get a VEV, two Weyl fermion doublets ψ_i^α (with

^{*}jeremie.choquette@physics.mcgill.ca

[†]jcline@physics.mcgill.ca

¹ For lower masses the DM self-interactions violate bounds from structure formation. This argument assumes that the DM remains ionized, which turns out to be valid for the gauge coupling strength needed to get the right relic density from thermal freezeout.

gauge index α and flavor index i) and the heavy right-handed neutrinos N_j that also interact in the usual way with the standard model neutrinos. An even number of fermion doublets is required to avoid Witten's global SU(2) anomaly [32]. They can be combined into a Dirac doublet fermion $\Psi = (\psi_{1L}, \psi_{2R}^c)$ where the conjugate is defined as $\psi_{2R}^c = \sigma_2 \tau_2 (\psi_{2L})^*$, *i.e.*, the epsilon tensor is applied both to the spin and to the SU(2)_h gauge indices. Without loss of generality the VEV of ϕ can be rotated to the 3rd component, $\langle \phi^a \rangle = (0, 0, \sigma)$.

particle VEV	$B^{0,+,--}$	$\phi^a \rightarrow$ (0, 0, $\sigma + \phi$)	$\eta^{+,-}$	$\Psi_1^{+,-}$	$\Psi_2^{+,-}$	N_j
Spin	1	0	0	$\frac{1}{2}$	$\frac{1}{2}$	$\frac{1}{2}$
SU(2) _h	3	3	2	2	2	1
U(1) _h	0, +2, -2	0	+1, -1	+1, -1	+1, -1	0

TABLE I: New particle content in the model, showing the Lorentz, hidden SU(2) and hidden U(1) (after breaking of SU(2)_h \rightarrow U(1)_h) quantum numbers.

The relevant terms in the Lagrangian are

$$\begin{aligned} \mathcal{L} = & -\frac{1}{4} B_{\mu\nu}^a B_a^{\mu\nu} + \frac{1}{2} (D_\mu \phi)^2 - \frac{1}{\Lambda} \phi^a B_{\mu\nu}^a Y^{\mu\nu} \quad (1) \\ & + \bar{\Psi} (i \not{D} - m_\psi) \Psi - \bar{\Psi} (y_1 + i y_2 \gamma_5) (\vec{\phi} \cdot \vec{\tau}) \Psi \quad (2) \\ & - |D_\mu \eta|^2 - V(H, \phi, \eta) \\ & - (\bar{\psi}_L^i \eta) y_\psi^{ij} P_R N_j + \text{h.c.} \end{aligned}$$

where the covariant derivative is $D_\mu \phi^a = \partial_\mu \phi^a - g \epsilon_{abc} B_\mu^b \phi^c$ or $D_\mu \Psi = (\partial_\mu - i(g/2) \vec{B}_\mu \cdot \vec{\tau}) \Psi$, g is the SU(2)_h gauge coupling, and $Y_{\mu\nu}$ is the Standard Model hypercharge gauge field strength. In the Yukawa interactions with the sterile neutrino we use the Weyl fermion notation since the analogy to leptogenesis via neutrino physics is more clear in this way.

The triplet scalar VEV breaks SU(2)_h to U(1)_h, mediated by the massless gauge boson B_3^μ , while $B^{\pm\pm} = (B^1 \pm i B^2)/\sqrt{2}$ obtain mass $m_B = g\sigma$. The upper and lower components $\Psi_{1,2}$ of the fermion doublet are also charged under the U(1)_h (with half the charge of $B^{\pm\pm}$). Their masses are split by the Yukawa interaction, $m_{1,2} = ((m_\psi \pm y_1 \sigma)^2 + (y_2 \sigma)^2)^{1/2}$. We used the freedom to perform a chiral rotation on Ψ so that m_ψ is real (has no γ_5 component).

In section 2.4 we discuss the decay of the scalars through $\eta \rightarrow \psi \nu$ via the dimension-5 operator

$$\bar{\psi}_{i,L} \eta y_\psi^{ij} M_j^{-1} y_\nu^{jk} P_R (H^T \bar{L}_k^T) + \text{h.c.} \quad (3)$$

where M_j is the heavy neutrino mass (in a basis where its mass matrix is diagonal), y_ν is the neutrino Yukawa matrix, H is the SM Higgs doublet, and L_k are the lepton doublets.

We will initially consider the case where decays $\Psi_1 \rightarrow B^{++} \Psi_2$ are not kinematically allowed. They would lead to a dark sector consisting of stable B^{++} vector bosons

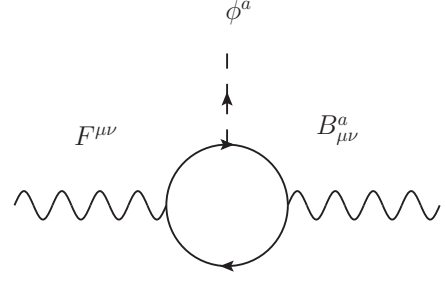


FIG. 1: Loop contribution to the nonabelian kinetic mixing operator.

and Ψ_2^- fermions. (The alternative case in which these decays are allowed is considered in section 4.) This leaves two species of stable dark matter, the Dirac fermions $\Psi_1 = (\psi_{1L}^1, \psi_{2R}^{2c})^T$ and $\Psi_2 = (\psi_{1L}^2, \psi_{2R}^{1c})^T$ with charges ± 1 under the unbroken U(1)_h. The long-range force mediated by the dark photon $B_3 \equiv \gamma'$ causes the symmetric component of the DM densities to be at least partially depleted by annihilations, and the asymmetric components of $\Psi_{1,2}$ to bind into dark atoms. The efficiency of these processes depends upon the gauge coupling g and the dark atom mass $m_{\mathbf{H}}$, as we will discuss in section 5.

For simplicity we impose a softly broken U(1) symmetry under which $\psi_i \rightarrow e^{i\theta} \psi_i$, $\eta \rightarrow e^{i\theta} \eta$, which forbids the interactions $(\bar{\psi}_i \tilde{\eta}) N_j$, with $\tilde{\eta} = \tau_2 \eta^*$. The symmetry is broken by the Dirac mass term, which takes the form

$$-m_\psi (\bar{\psi}_{2R}^{2c} \psi_{1L}^1 + \bar{\psi}_{2R}^{1c} \psi_{1L}^2) + \text{h.c.} \quad (4)$$

If the symmetry were exact, then the subsequent decays $\eta \rightarrow \psi$ mediated by N_i would completely erase any produced DM asymmetry. However the chirality flips induced by the mass term prevent this erasure, as we will explain in more detail in section 2. There is an unbroken discrete Z_2 remnant of this symmetry, where $\psi_i \rightarrow -\psi_i$ and $\eta \rightarrow -\eta$, that ensures the stability of the dark matter.

The potential V is assumed to give rise to the VEV of ϕ and it generically also includes the Higgs portal coupling $\frac{1}{2} \lambda_{h\phi} |H|^2 \phi^2$. Once ϕ gets its VEV, the nonabelian kinetic mixing operator can be written as

$$-\frac{1}{2} \sin \tilde{\epsilon} B_{\mu\nu}^3 Y^{\mu\nu} \quad (5)$$

where $\sin \tilde{\epsilon} = 2\sigma/\Lambda$. It could arise from integrating out a heavy vector-like fermion χ that carries hypercharge and transforms as a doublet under SU(2)_h. The interaction $y_\chi \bar{\chi} \phi_a \sigma_a \chi$ leads to the diagram in fig. 1, implying $\Lambda^{-1} \sim gg_1 y_\chi / m_\chi$ where g_1 is the hypercharge coupling. The kinetic mixing gives rise to electric millicharges $\pm \tilde{\epsilon} g \equiv \pm \epsilon e$ for the fermions $\Psi_{1,2}$. This or alternatively the Higgs portal interaction allows for direct detection of the dark atoms, as we discuss in section 3.

2. ORIGIN OF DARK MATTER ASYMMETRY

Our setup allows for heavy neutrinos to decay in a CP-violating manner into an excess of dark matter versus its antiparticles in close analogy to leptogenesis. The structure of Yukawa couplings is similar to that of neutrinos except that we have only two light fermionic DM species, $\Psi_{1,2}$ as compared to the three light neutrinos. The dark Higgs doublet η does not have a VEV, so it also gets an asymmetry, which will be determined by those in Ψ_i .

The asymmetry in the decay of the j th heavy neutrino into $\psi_i^* \eta$ versus $\psi_i \eta^*$ (recall that ψ_i denotes the Weyl doublet states) is given by

$$\begin{aligned} \epsilon_{\psi}^{ji} &= \frac{\Gamma(N_j \rightarrow \psi_i^* \eta) - \Gamma(N_j \rightarrow \psi_i \eta^*)}{\Gamma(N_i \rightarrow \text{any})} \\ &= \frac{1}{8\pi} \sum_{k \neq j} \left[\frac{\text{Im} \left[(y_{\psi}^{\dagger} y_{\psi})_{kj} y_{\psi}^{ik} y_{\psi}^{ij*} \right]}{(y_{\psi}^{\dagger} y_{\psi} + y_{\nu}^{\dagger} y_{\nu})_{jj}} g(M_k^2/M_j^2) \right. \\ &\quad \left. + \frac{\text{Im} \left[(y_{\nu}^{\dagger} y_{\nu})_{kj} y_{\psi}^{ik} y_{\psi}^{ij*} \right]}{(y_{\psi}^{\dagger} y_{\psi} + y_{\nu}^{\dagger} y_{\nu})_{jj}} g'(M_k^2/M_j^2) \right] \end{aligned} \quad (6)$$

where $g(x) = \sqrt{x} [1/(1-x) + 1 - (1+x) \ln(1+1/x)]$ and $g'(x) = \sqrt{x}/(1-x)$. This differs from the standard leptogenesis expression because the denominator must take into account decays of N_j both into neutrinos and dark matter, and there is a mixed term of order $y_{\nu}^2 y_{\psi}^2$ from the self-energy correction of N_j by the SM Yukawa interaction.

For definiteness, we will focus on decay of the lightest heavy neutrino N_1 . In the simplest scenario of leptogenesis, where $M_1 \ll M_{2,3}$ and the reheat temperature is in between, $M_1 < T_{rh} < M_{2,3}$, this is the only relevant decay since the heavier neutrinos are not present. In this case the functions in eq. (6) can be approximated as $g \cong -3/2\sqrt{x}$ and $g' \cong -1/\sqrt{x}$ with $x = (M_2/M_1)^2 \gg 1$.

Initially, we can expect independent asymmetries $Y_{1,2}$ for ψ_1 and ψ_2 , where $Y_i = (n_{\psi_i} - n_{\bar{\psi}_i})/s$ is the dark matter to entropy ratio, since $\epsilon_{\psi}^{11} \neq \epsilon_{\psi}^{12}$. However the Dirac mass term takes the form $\psi_1^T \sigma_2 \tau_2 \psi_2$, which implies that mass effects will cause the asymmetries of ψ_1 and ψ_2 to become equal and opposite. This projects the net asymmetry of the fermions onto the difference between the initial ones, $Y_{\psi} = Y_1 - Y_2$, at temperatures where the helicity-flipping interactions due to m_{ψ} come into equilibrium.

On the other hand, the η boson gets a different asymmetry, proportional to $\epsilon_{\psi}^{11} + \epsilon_{\psi}^{12}$. Eventually it will decay into ψ_i . For simplicity, we consider the case $\epsilon_{\psi}^{11} \sim -\epsilon_{\psi}^{12}$. Then not only does the initial asymmetry in η tend to be small, but so also is its contribution to the final asymmetry in ψ_i , and we can estimate the net asymmetry in ψ from N_1 decays as

$$\epsilon_{\psi 1} \sim \epsilon_{\psi}^{11} - \epsilon_{\psi}^{12} \sim 2\epsilon_{\psi}^{11} \quad (7)$$

The sign difference is in contrast to the CP asymmetries

for decays into neutrinos, $\epsilon_{\nu 1} = \sum_i \epsilon_{\nu}^{1i}$ familiar from leptogenesis.

2.1. Dark matter asymmetry estimate

The initial asymmetries depend upon an efficiency factor κ_{ψ} that quantifies the amount of washout (see for example [33] for a review). The contribution from N_1 decay is

$$Y_{\psi} = \frac{45}{\pi^4} \frac{\epsilon_{\psi 1} \kappa_{\psi}}{g_*} \quad (8)$$

where $\kappa_{\psi} \cong \min(0.25 (m_*/\tilde{m}_{\psi 1})^{1.1}, 1)$ with $\tilde{m}_{\psi 1} = 2(y_{\psi}^{\dagger} y_{\psi})_{11} v^2/M_1$, $m_* = 10^{-3} \text{ eV}$ and $v = 174 \text{ GeV}$. The Higgs VEV v has no direct physical relevance for the dark matter abundance, but $\tilde{m}_{\psi 1}/m_*$ gives $\Gamma(N_1 \rightarrow \psi \eta^{(*)})/H(M_1)$ (the ratio of the partial decay width to the Hubble rate), just like $\tilde{m}_{\nu 1}/m_*$ does for the decays into νh . The dark sphalerons associated to the $SU(2)_h$ gauge interactions have the same effect as (an increase in) the Dirac mass term for Ψ and therefore do not require additional consideration for the dark asymmetry.

If there is no hierarchical structure to the couplings y_{ψ}^{ij} and their phases are large, we can estimate $(y_{\psi}^{\dagger} y_{\psi})_{kj} \sim (\tilde{y}_{\psi}^{\dagger} \tilde{y}_{\psi})_{kj}$ or its imaginary part by some average value \bar{y}_{ψ}^2 . Further defining $\bar{y}_{\nu}^2 = (y_{\nu}^{\dagger} y_{\nu})_{11}$ and assuming that the terms of order y_{ν}^2 in the numerator of (6) can be estimated as \bar{y}_{ν}^2 , we find that the CP asymmetry for ψ is of order

$$\epsilon_{\psi 1} \sim \frac{2 \bar{y}_{\psi}^2}{8\pi \sqrt{x}} \left(\frac{1 + \frac{3}{2}r}{1+r} \right) \quad (9)$$

where we define $r = \bar{y}_{\psi}^2/\bar{y}_{\nu}^2$, and assume that $\epsilon_{\psi}^{12} \sim -\epsilon_{\psi}^{11}$ in (8). It is evident that eq. (9) has only mild dependence upon r . Combining with the efficiency factor κ_{ψ} (where we approximate the exponent 1.1 by 1) leads to the estimate²

$$Y_{\psi} \cong 1.4 \times 10^{-12} \left(\frac{M_1}{10^{10} \text{ GeV}} \right) \left(\frac{10}{x^{1/2}} \right) \quad (10)$$

ignoring r dependence.

2.2. Baryon asymmetry estimate

We wish to explain the baryon asymmetry simultaneously with that of dark matter. Analogously to (8), it is

² This is valid for parameters such that $\kappa_{\psi} < 1$ hence $\tilde{m} \gtrsim 4m_*$. Using eq. (13) this implies $\bar{y}^2 \gtrsim 10^{-7} (M_1/10^{10} \text{ GeV})$. We will assume that this restriction holds in the following.

given by

$$Y_B = \frac{28}{79} \cdot \frac{45}{\pi^4} \frac{\epsilon_{\nu,1} \kappa_\nu}{g_*} \quad (11)$$

where the prefactor 28/79 is due to redistribution of the initial lepton asymmetry into baryons via sphaleron interactions. The CP asymmetry $\epsilon_{\nu,1}$ is defined as $\epsilon_{\nu,1} = \sum_i \epsilon_{\nu,1i}$ in the usual way for leptogenesis. Similarly to our estimate in (9), we expect the well-known D-I bound [34] to be modified by a function of $r = \bar{y}_\psi^2/\bar{y}_\nu^2$,

$$\begin{aligned} |\epsilon_{\nu,1}| &\leq \frac{3}{16\pi} \frac{M_1}{v^2} \frac{\Delta m_{\text{atm}}^2}{m_{\nu_3}} \left(\frac{1 + \frac{2}{3}r}{1+r} \right) \\ &\cong 10^{-6} \left(\frac{M_1}{10^{10} \text{ GeV}} \right) \equiv 10^{-6} M_{10} \end{aligned} \quad (12)$$

where $\Delta m_{\text{atm}}^2 = m_{\nu_3}^2 - m_{\nu_2}^2$, which we assume to be $\cong m_{\nu_3}^2 \cong (0.05 \text{ eV})^2$. Again the dependence upon r is mild, and we will ignore the effect of the DM Yukawa coupling on leptogenesis in the visible sector. To estimate the efficiency factor $\kappa_\nu \cong 0.25 (m_*/\tilde{m}_\nu)$, with $\tilde{m}_\nu = (y_\nu^\dagger y_\nu)_{11} v^2/M_1$, we use the Casas-Ibarra parametrization of y_ν ,

$$\begin{aligned} (y_\nu^\dagger y_\nu)_{11} &\cong U_{1i} m_{\nu_i}^{1/2} R_{ik}^\dagger \frac{M_k}{v^2} R_{kj} m_{\nu_j}^{1/2} U_{j1}^\dagger \\ &\cong 10^{-6} M_{10} \end{aligned} \quad (13)$$

(the same result as eq. (12)) where U is the PMNS matrix and R is an arbitrary SU(3) transformation. We assumed that $R_{ik}^\dagger M_k R_{kj} \sim M_1$ since we take the heavy neutrino masses to be of the same order, and $|U_{12}|^2 m_{\nu_2} + |U_{13}|^2 m_{\nu_3} = 0.003 \text{ eV}$ (taking m_{ν_1} to be much less than the solar neutrino mass splitting). This gives $\kappa_\nu \cong 1/12$ and

$$Y_B \cong 1.4 \times 10^{-10} M_{10} \epsilon_{\text{DI}} \quad (14)$$

where we have introduced a parameter ϵ_{DI} to quantify how much $\epsilon_{\nu,1}$ falls below the D-I bound, *i.e.*, ϵ_{DI} is $|\epsilon_{\nu,1}|$ over its maximum value. Equating Y_B to its measured value, we find $\epsilon_{\text{DI}} M_{10} = 0.7$.

2.3. DM to baryon constraint

We can combine the above results to get a constraint on the model parameters from the known ratio of baryon and dark matter energy densities, $\Omega_B/\Omega_{DM} = m_p Y_B / (m_{\text{H}} Y_\psi) = 0.18$. Here $m_{\text{H}} = m_1 + m_2$, the mass of the dark atom (neglecting its binding energy). Then we find $m_{\text{H}}/m_p = 166 \epsilon_{\text{DI}} (x/10)^{1/2}$. We can eliminate ϵ_{DI} using eq. (14) and M_1 using (13) to obtain

$$\frac{m_{\text{H}}}{m_p} = 560 \epsilon_{\text{DI}} \left(\frac{x^{1/2}}{10} \right) = \frac{360}{M_{10}} \left(\frac{x^{1/2}}{10} \right) \quad (15)$$

Eq. (15) reveals part of our motivation for the choice $M_1 \sim 10^{10} \text{ GeV}$: it gives dark atom masses in a range that

is interesting for direct detection and consistent with our prejudice for the new physics scale to not be far below the weak scale. It is interesting that the same mass scale is also consistent with the observed baryon asymmetry for generic choices of the neutrino CP asymmetry, $\epsilon_{\text{DI}} \lesssim 1$.

Notably absent from our estimates is any explicit dependence upon the Yukawa couplings \bar{y}_ψ^2 and \bar{y}_ν^2 . This is because of the cancellation between the CP asymmetry ϵ and the efficiency factor κ , which only occurs for couplings such that $\kappa < 1$. We verified this condition for $\kappa_\nu = 0.08$. It is also satisfied by κ_ψ so long as $\bar{y}_\psi^2 \gtrsim \bar{y}_\nu^2/12$. We will make this technical assumption to keep the analysis simple. For smaller values of \bar{y}_ψ^2 , there would be a suppression of Y_ψ and the need for correspondingly larger values of m_{H} .

As an example, we take $\epsilon_{\text{DI}} = 0.65$, $\bar{y}_\psi^2 = \bar{y}_\nu^2 = 10^{-6}$, $m_{\text{H}} \cong 83 \text{ GeV}$, $M_1 = 10^{10} \text{ GeV}$, $M_2 = \sqrt{x} M_1 = 2 \times 10^{11} \text{ GeV}$. Larger or smaller values of m_{H} can be obtained by adjusting M_2/M_1^2 , using eq. (15).

2.4. Decay of dark scalars

An interesting feature of our model is that the seesaw mechanism produces the new dimension-5 operator (3) that allows the dark scalars η to decay [29]. When the SM Higgs takes its vacuum expectation value, this allows the η to decay directly into $\nu\psi$. The decay rate is of order

$$\Gamma \sim \frac{\bar{y}_\psi^2 \bar{y}_\nu^2 m_\eta v^2}{8\pi M_1^2} \quad (16)$$

$$\sim 3 \times 10^{-3} \text{ s}^{-1} \cdot \left(\frac{m_\eta}{150 \text{ GeV}} \right) \quad (17)$$

where for the numerical estimate of Γ we used the exemplary values specified at the end of the previous section (ignoring the mass of ψ in the phase space integral).

Such decays must occur sufficiently early so that the decay products are fully thermalized before they can distort the CMB. Ref. [35] shows that this occurs if the lifetime is below $\sim 10^{12} \text{ s}$. Eq. (16) implies that our model easily satisfies this bound.

3. DIRECT DETECTION

There are two portals through which our dark atoms to interact with nuclei. The kinetic mixing allows for photon exchange, which has been discussed in refs. [21, 22]. The ensuing constraints on the electric millicharge ϵ are weakened for atoms compared to ions because of the screening of electric charge. In the special case where $m_1 = m_2$ this screening is perfect, and the interaction becomes magnetic dipole, further weakening the limits [17]. Here we extend results of ref. [17] for the $m_1 = m_2$ case to higher DM masses.

In addition, there is the Higgs portal induced by mixing of h and ϕ_3 through the operator $\frac{1}{2} \lambda_{h\phi} |H|^2 |\phi|^2$. ϕ_3

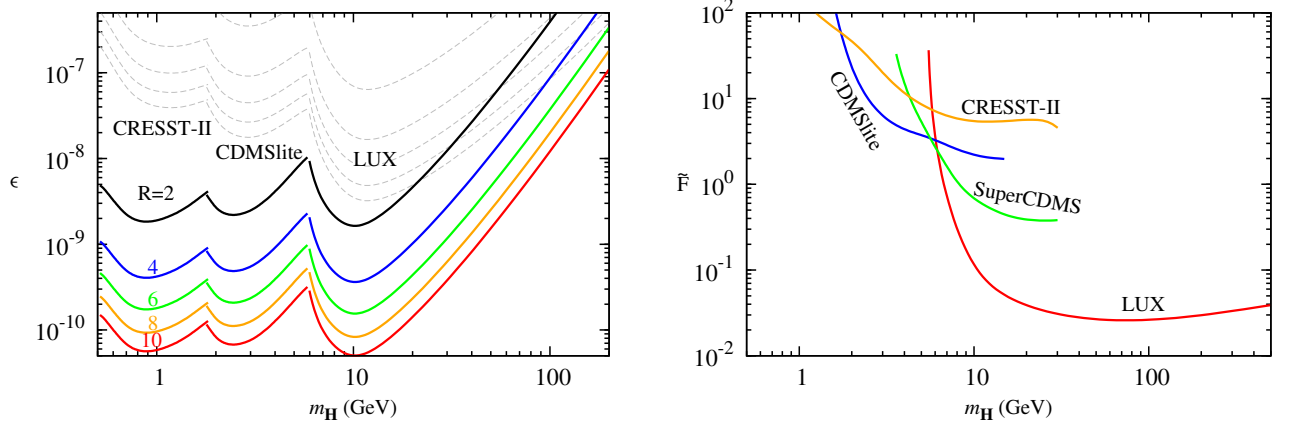


FIG. 2: Left: CRESST-II, CDMSlite and LUX limits on millicharge ϵ of dark atom constituents, with constituent mass ratios $m_2/m_1 = R = 2, 4, \dots, 10$ as indicated, for photon-mediated scattering of dark atoms on protons. For clarity, only the most constraining limit is shown for any DM atom mass m_H . Gauge coupling is set to $\alpha_g = \alpha_{\text{ion}}$, eq. (19) for solid curves, and fixed at $\alpha_g = 0.06$ for light dashed curves. Right: Corresponding limits on $\tilde{F} = y_1 \theta |1 - m_h^2/m_\phi^2| F_\psi(0)$ from Higgs portal scattering, where θ is the ϕ -Higgs mixing angle.

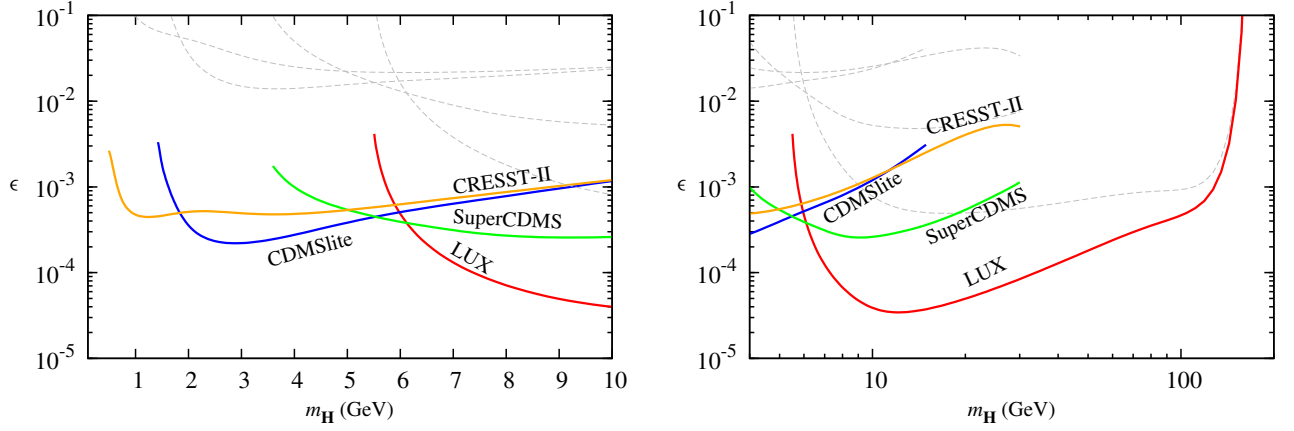


FIG. 3: Direct detection constraints on kinetic mixing parameter ϵ versus dark atom mass m_H for case of equal-mass constituents $m_1 = m_2 = m_H/2$, when interaction is magnetic inelastic. Hyperfine mass splitting is chosen as a function of m_H as described in text. Solid and dashed curves refer to choice of α_g as in fig. 2. Left: low mass region; right: larger mass region.

interacts with the dark atom constituents through the operator $\bar{\Psi}(y_1 + iy_2 \gamma_5)(\vec{\phi} \cdot \vec{\tau})\Psi$ that splits the $\Psi_{1,2}$ masses.

3.1. Kinetic mixing portal

3.1.1. Unequal-mass constituents

As discussed in ref. [21], the mutual screening of the electric charges of the Ψ_1 and Ψ_2 constituents results in a scattering matrix element where the $1/q^2$ of the photon propagator is canceled by q^2 in the form factor for the charge density. The cross section for scattering of dark

atoms on a proton is

$$\begin{aligned} \sigma_p &= 4\pi \frac{\alpha^2 \epsilon^2 \mu_n^2}{\alpha_g^4} \left(\frac{1}{m_1^2} - \frac{1}{m_2^2} \right)^2 \\ &= 4\pi \frac{\alpha^2 \epsilon^2 \mu_n^2}{\alpha_g^4 m_H^4} f_0(R) \end{aligned} \quad (18)$$

where μ_n is the reduced mass of the dark atom and nucleon system, and $f_0(R) = (1 + 1/R)^4 (R^2 - 1)^2$. Here we have generalized the result of ref. [21] where the approximation of large R was made. The expression (18) is valid if R is not too close to 1. The question of “how close?” is discussed below.

For $R \neq 1$, the resulting upper limits on ϵ is illustrated in fig. 2(a) showing the most constraining limit from the LUX [36], CRESST-II [37] or CDMSlite [38] experiments,

at any given dark atom mass $m_{\mathbf{H}}$. In section 5 we will see that the requirement of sufficiently small ionization fraction in the dark sector leads to the constraint

$$\alpha_g \geq \alpha_{\text{ion}} \equiv 5 \times 10^{-3} \left(\frac{m_{\mathbf{H}}}{\text{GeV}} \right)^{1/2} f_2^{-1/4}(R) \quad (19)$$

where

$$f_2(R) = R + 2 + R^{-1} \quad (20)$$

The solid curves are derived for the parameter choice which saturates this bound, $\alpha_g = \alpha_{\text{ion}}$, and R ranging from 2 to 10, while the dashed ones assume a fixed value of $\alpha_g = 0.06$. This value satisfies the constraint $\alpha_g > \alpha_{\text{ion}}$ over the entire range of R and $m_{\mathbf{H}}$ shown on the plots. (The unusual sensitivity of the solid curves to light DM masses is due to the decrease of $\alpha_g = \alpha_{\text{ion}}$ with $m_{\mathbf{H}}$, and consequent increase in the dark Bohr radius, leading to larger cross sections.) The nominal constraints from the experiments are weakened by factors of $(A/Z)^2 = 5.9, 5.2$ and 4 respectively to account for the coupling to protons only. For CRESST this corresponds to collisions with the oxygen atoms that dominate the sensitivity to low-mass dark matter. The strongest constraints occur for $m_{\mathbf{H}} \cong 1 - 10 \text{ GeV}$, in the range $\epsilon \lesssim 10^{-10} - 10^{-8}$. For conventional abelian kinetic mixing, such small values of ϵ could be difficult to achieve since the loop diagram that generates it is not suppressed by any large mass scales, since in this case the kinetic mixing operator is marginal. However for nonabelian kinetic mixing, ϵ is suppressed by the mass m_χ of the heavy particle in the loop, as well as its Yukawa coupling y_χ . For example if the couplings described below eq. (5) are $y_\chi = 0.1$, $g_1 = g$, $R = 10$, $\alpha_g = \alpha_{\text{ion}}$ and $\sigma = 30 \text{ GeV}$, we require $m_\chi \gtrsim 3 \times 10^{11} \text{ GeV}$ to satisfy the LUX bound on 10 GeV dark atoms.

3.1.2. Equal-mass constituents

For $R \cong 1$, there is perfect screening of charge because of the complete overlap of the wave functions of the two constituents, and the magnetic dipole interaction that we have neglected in (18) becomes important. This case was considered in detail in ref. [21]. The magnetic scattering is inelastic because of the hyperfine transition of the dark atom, requiring energy $\delta E = \frac{1}{6} \alpha_g^4 m_{\mathbf{H}}$, hence a minimum DM velocity of $v_{\text{min}} = q/(2\mu_N) + \delta E/q > \sqrt{2\delta E/\mu_N}$ for momentum transfer q and dark atom-nucleus reduced mass μ_N . There is a q - and v -dependent form factor $F = (q_0/q)^2 (v^2 - v_{\text{min}}^2)/v_0^2$ that is of order unity for typical values $v \sim v_0$ and $q \sim q_0$, as long as $v_0 \gtrsim v_{\text{min}}$. The cross section on protons is of order

$$\sigma_{p,0} \equiv \frac{64\pi\epsilon^2\alpha^2\mu_n^2v_0^2}{m_{\mathbf{H}}^2q_0^2} \quad (21)$$

in that case, where μ_n is the proton-atom reduced mass.

More quantitatively, the actual cross section for a given scattering event is $\sigma_p = \sigma_{p,0} F(q, v)$ and the detection rate is proportional to

$$R \propto Z^2 \int_{E_{\text{min}}}^{E_{\text{max}}} dE_R \int_{v_{\text{min}}}^{v_{\text{esc}}} \frac{d^3\vec{v}}{v} f(\vec{v}) \sigma_p \quad (22)$$

$$\propto Z^2 \sigma_{p,0} I_F, \quad (23)$$

with

$$\begin{aligned} E_{\text{min}} &= \frac{1}{2} m_{\mathbf{H}} v_{\text{min}}^2 \\ E_{\text{max}} &= p_{\text{max}}^2 / (2m_N) \\ p_{\text{max}} &= \sqrt{\mu_n^2 (v_{\text{esc}} + v_0)^2 - 2\delta E \mu_N + \mu_N (v_{\text{esc}} + v_0)} \\ f(\vec{v}) &\propto e^{-(\vec{v} + \vec{v}_e)^2 / v_0^2} - e^{-v_{\text{esc}}^2 / v_0^2}, \end{aligned} \quad (24)$$

$$I_F \equiv \int_{E_{\text{min}}}^{E_{\text{max}}} dE_R \int_{v_{\text{min}}}^{v_{\text{esc}}} \frac{d^3\vec{v}}{v} f(\vec{v}) F(q, v). \quad (25)$$

Here \vec{v}_e is the Earth's speed relative to the DM halo, $v_0 \approx 220 \text{ km s}^{-1}$ is the mean DM velocity, $v_{\text{esc}} \approx 450 \text{ km s}^{-1}$ is the approximate escape velocity of the DM halo (we see no significant variation in the results for values in the range $400 - 500 \text{ km s}^{-1}$), and E_{esc} is the maximum recoil energy from a DM particle with the escape velocity.

We compare the rate for our model to that of generic DM scattering with a constant cross section σ_n , for which the corresponding expressions are

$$R \propto A^2 \sigma_n I_0, \quad (26)$$

$$I_0 \equiv \int_{E_{\text{min}}}^{E_{\text{max}}^{(0)}} dE_R \int_{v_{\text{min}}}^{v_{\text{esc}}} \frac{d^3\vec{v}}{v} f(\vec{v}). \quad (27)$$

where $E_{\text{max}}^{(0)} = E_{\text{max}}$ evaluated at $\delta E = 0$. Therefore the magnetic inelastic cross section (21) is bounded from above as

$$\sigma_{p,0} < \frac{A^2 I_0}{Z^2 I_F} \sigma_{n,\text{lim}} \quad (28)$$

where $\sigma_{n,\text{lim}}$ is the experimental upper limit on the cross section for a generic DM model. Notice that the arbitrary quantity $(v_0/q_0)^2$ appears in the same way on both sides of (28) and hence can be divided out.

Although the gauge coupling α_g does not appear in (21), the mass splitting $\delta E = \alpha_g^4 m_{\mathbf{H}}/6$ depends upon it. For definiteness, we have chosen the value $\alpha_g = \alpha_{\text{ion}}$ in eq. (19) from the requirement of sufficiently small dark ionization fraction. This fixes δE as a function of $m_{\mathbf{H}}$.

We plot the ensuing limits on ϵ in figure 3, using results from the LUX [36], SuperCDMS [39], CRESST-II [37], and CDMSlite [38] experiments. The mass dependence of $\alpha_g = \alpha_{\text{ion}}$ changes the shape of the exclusion curves relative to those on the cross section itself, since the mass splitting δE rises rapidly with $m_{\mathbf{H}}$, nullifying the signal for $m_{\mathbf{H}} \gtrsim 100 \text{ GeV}$.

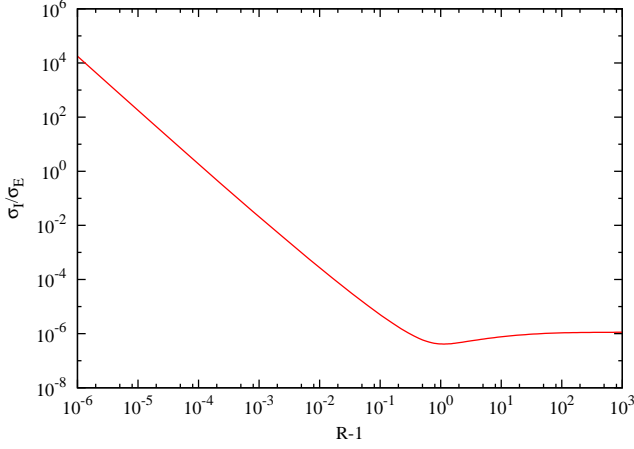


FIG. 4: Ratio of the magnetic inelastic and elastic cross section for scattering of dark atoms on protons as a function of the constituent mass ratio R (its deviation from unity), for dark atom mass $m_{\mathbf{H}} = 10$ GeV and mass splitting described in section 3.1.2.

3.1.3. Transition from $R = 1$ to $R > 1$

We have noted that inelastic magnetic transitions dominate for equal constituent masses, $R = 1$, while elastic charge-charge interactions dominate when $R > 1$. One may wonder how sharp the transition is between the two regimes; how small must $R - 1$ be for inelastic transitions to dominate? We have calculated the ratio of the two cross sections as a function of R for a particular value of $m_{\mathbf{H}} = 10$ GeV as an example, taking the mass splitting δE as described above. The result is graphed in fig. 4, which shows that only for $R < 1.0001$ do the inelastic transitions dominate. Hence the most natural situation corresponding to this case is that where $R = 1$ exactly. There are two limits in our model that give $R = 1$: either $y_1 = 0$, or $m_\psi = 0$. The latter is a point of enhanced SU(2) flavor symmetry for the two chiral (doublet) fermions.

3.2. Higgs portal

The interaction of dark atoms with the Higgs through ϕ_3 - H mixing also undergoes screening because of the coupling τ_3 which has opposite sign for Ψ_1 and Ψ_2 . At low energies, the dark atoms can be described by a Dirac field \mathbf{H} whose coupling to the virtual ϕ_3 or h carrying momentum q is given by the amplitude

$$y_1 \bar{u}_{\mathbf{H}} u_{\mathbf{H}} F_\psi(q) \quad (29)$$

We have neglected the y_2 contribution that is suppressed by the dark matter velocity. By matching onto the scattering amplitudes in the high-energy theory, we infer that

$$F_\psi(q) = \frac{1}{m_{\mathbf{H}}} \left[\frac{m_2}{(1 + \frac{1}{4}q^2 a_2^2)^2} - \frac{m_1}{(1 + \frac{1}{4}q^2 a_1^2)^2} \right] \quad (30)$$

with $a_i = (\alpha_g m_i)^{-1}$. Thus the coupling vanishes in the limit $R = 1$ ($m_1 = m_2$). If θ is the h - ϕ_3 mixing angle, then the amplitude for scattering of dark atoms on nucleons is

$$\mathcal{M} = y_1 \bar{u}_{\mathbf{H}}(p_3) u_{\mathbf{H}}(p_1) \cdot \bar{u}_n(p_4) u_n(p_2) \left(\frac{y_n m_n}{v} \right) \quad (31)$$

$$\times c_\theta s_\theta \left(\frac{1}{m_h^2} - \frac{1}{m_\phi^2} \right) F_\psi(q)$$

where $(y_n m_n/v)$ with $y_n \cong 0.3$ [40] is the coupling of the Higgs to nucleons.

If α_g is not too small, we can take the $q = 0$ limit of the form factor. In this case the cross section for dark atom-nucleon scattering is

$$\sigma_n \cong \frac{1}{\pi v^2} [y_1 y_n m_n \mu_{n\mathbf{H}} \theta F_\psi(0)]^2 (m_\phi^{-2} - m_h^{-2})^2 \quad (32)$$

in terms of the \mathbf{H} -nucleon reduced mass, and taking $\theta \ll 1$. The LUX upper limit on the dimensionless combination $\tilde{F} = y_1 \theta [1 - m_h^2/m_\phi^2] F_\psi(0)$ is plotted in fig. 2. The Yukawa coupling y_1 is related to the mass splitting in the dark sector since $m_2^2 - m_1^2 = y_1^2 \sigma^2$. Moreover it is straightforward to show that $F_\psi(0) = (m_2^2 - m_1^2)/m_{\mathbf{H}}^2$. If $m_\phi < m_h$ then $\tilde{F} \cong y_1^3 \theta (m_h^2 \sigma^2)/(m_\phi^2 m_{\mathbf{H}}^2)$. We expect $m_\phi \sim \sigma$, similarly to $m_h \sim v$ in the visible sector, and $\theta \lesssim 0.01$ to satisfy LEP constraints [41] on mixing of a light scalar with the Higgs. The largest dark atom mass range for saturating the LUX bound shown in fig. 2 with $|y_1| \lesssim 1$ is $m_{\mathbf{H}} \lesssim 70$ GeV.

4. STABLE VECTOR BOSONS

Up to now we have assumed that the Ψ_1 - Ψ_2 mass splitting is sufficiently small to prohibit the decay $\Psi_2^- \rightarrow B^{--} \Psi_1^+$, corresponding to the condition

$$|y_1| < \frac{m_1 + m_2}{4m_\psi} g \quad (33)$$

However this need not be the case, and the model is also compatible with a universe where charge neutrality in the dark sector is achieved by having two Ψ_1^+ particles for every B^{--} . This leads to a very different kind of dark atom that is reminiscent of the H_2 molecule, except that the two “protons” are bound together by a single charge -2 “electron”. We will refer to these variant dark atoms as \mathbf{H}_2 . In the absence of fine-tuning, the stable vector boson is typically lighter than Ψ_1 , prompting us to define the ratio

$$R_2 = \frac{m_1}{m_B} \geq 1 \quad (34)$$

in analogy to $R = m_2/m_1$ for \mathbf{H} atoms.³

³ To get the opposite situation where $m_B > m_1$, we need $(g\sigma)^2 > (m_\psi - y_1\sigma)^2 + (y_2\sigma)^2$. This requires not only y_2 to be small, but also an accidental cancellation between m_ψ and $y_1\sigma$.

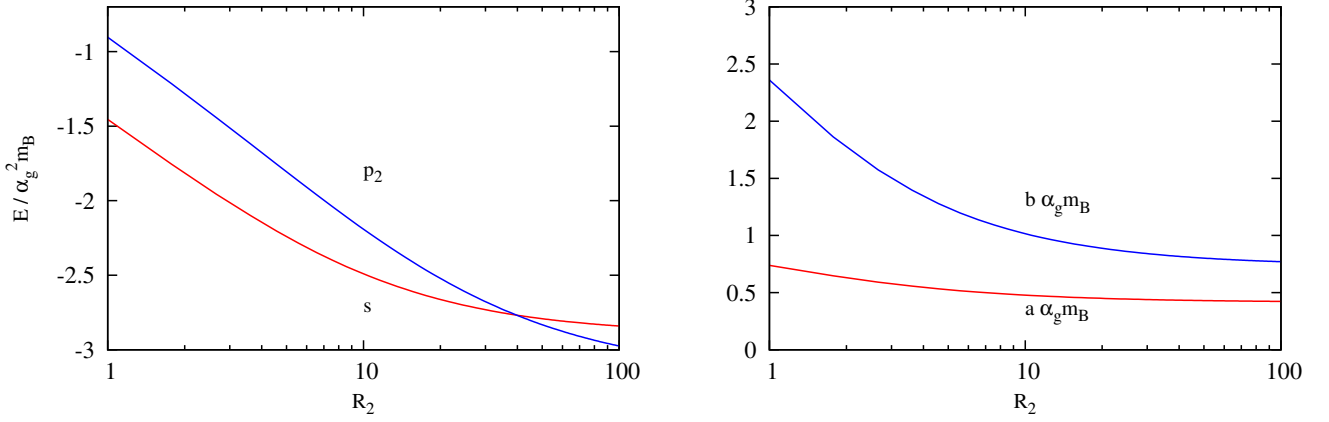


FIG. 5: Left: energy obtained from variational method as a function of R_2 for the trial wavefunctions for \mathbf{H}_2 bound states $\psi_{\mathbf{H}_2,s}$ and $\psi_{\mathbf{H}_2,p2}$. Right: Corresponding values of the parameters a, b (shown in dimensionless combinations with $\alpha_g m_B$) that determine the spatial distributions of the wave functions, for the s -wave.

4.1. Bound States

To verify the existence of the 3-body \mathbf{H}_2 bound states, we make some ansätze for its wave function and use the variational method to prove that the energy is minimized at a negative value. We consider trial wave functions where the positions of the three particles are given by

$$\vec{x}_\psi = \pm \vec{\Delta}/2, \quad \vec{x}_B = \vec{r} \quad (35)$$

i.e., we work in the center-of-mass frame of the two Ψ_1 particles, with $\vec{\Delta}$ being their relative separation. In analogy to the H_2 molecule, it could be expected that the wavefunction for Δ is approximately that of a 3D harmonic oscillator, $e^{-\Delta^2/b^2}$ for some scale b . For simplicity we take the wave function for r to be hydrogen-like, $e^{-r/a}$ for some other scale a . We consider three possible states, an s -wave and two p -waves,

$$\begin{aligned} \psi_{\mathbf{H}_2,s}(\vec{r}, \vec{\Delta}) &= N_s e^{-\Delta^2/b^2 - r/a} \\ \psi_{\mathbf{H}_2,p1}(\vec{r}, \vec{\Delta}) &= N_{p1} r_z e^{-\Delta^2/b^2 - r/a} \\ \psi_{\mathbf{H}_2,p2}(\vec{r}, \vec{\Delta}) &= N_{p2} \Delta_z e^{-\Delta^2/b^2 - r/a} \end{aligned} \quad (36)$$

where r_z (Δ_z) is the z -component of \vec{r} ($\vec{\Delta}$).

It is convenient to work in the analog of atomic units by rescaling to dimensionless coordinates $r = r'/(\alpha_g m_B)$, $\Delta = \Delta'/(\alpha_g m_B)$. Then the Hamiltonian can be written as $H = (\alpha_g^2 m_B) H'$, where the dimensionless H' is

$$H' = -\frac{1}{R_2} \nabla_{\Delta'}^2 - \frac{1}{2} \nabla_{r'}^2 + \frac{1}{\Delta'} - \sum_{\pm} \frac{2}{|\vec{r}' \pm \vec{\Delta}'/2|}. \quad (37)$$

By minimizing the expectation values $E = \langle \psi_{\mathbf{H}_2} | H | \psi_{\mathbf{H}_2} \rangle$ with respect to a, b and varying over a range of R_2 values, we find that bound states (having $E < 0$) exist for all three trial wave functions, but

$\Psi_{\mathbf{H}_2,p1}$ is always more weakly bound than the other two. Moreover the s -wave has lower energy than $p2$ only for $R_2 \lesssim 40$; for $R_2 > 40$ the $p2$ state is lower, as shown in fig. 5. Taking as an example the values $m_1 = 60 \text{ GeV}$, $R_2 = 10$, $\alpha_g = 3 \times 10^{-2}$, the three-constituent atoms have binding energies of approximately $E \approx -15 \text{ MeV}$.

4.2. Direct Detection

Dark \mathbf{H}_2 atoms interact similarly with nucleons relative to our treatment for \mathbf{H} atoms in section 3, but there are some qualitative differences, due to the more complicated wave function. In particular, there is no longer any special case like $R = 1$ for \mathbf{H} atoms in which the electric millicharge clouds of the constituents give exactly canceling contributions to the total charge density. This can be seen by computing the form factor, which is the Fourier transform of the charge density

$$\begin{aligned} \rho(x) &= \int d^3 \Delta d^3 r |\Psi(\vec{r}, \vec{\Delta})|^2 \\ &\times \left(\sum_{\pm} \delta(\vec{x} \pm \vec{\Delta}/2) - 2\delta(\vec{x} - \vec{r}) \right) \end{aligned} \quad (38)$$

Using $\psi_{\mathbf{H}_2,s}$ from eq. (36), the form factor is

$$\begin{aligned} F(q) &= 2 \left(-e^{-b^2 q^2/32} + \frac{1}{(1 + a^2 q^2/4)^2} \right) \\ &\cong q^2 \left(\frac{b^2}{16} - a^2 \right), \end{aligned} \quad (39)$$

where the approximation is for low momentum transfer q .

In computing the cross section for scattering on protons, the factor of q^2 in the form factor cancels the $1/q^2$

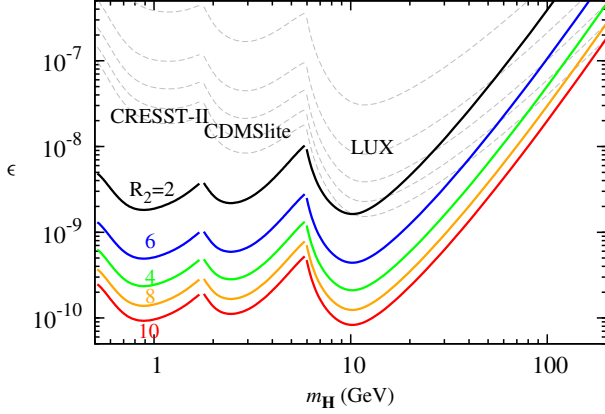


FIG. 6: Direct detection constraints on kinetic mixing parameter as in fig. 2, but for \mathbf{H}_2 atoms with $m_1/m_B \equiv R_2 = 2, 4, \dots, 10$.

of the propagator like before, giving

$$\sigma_p = 16\pi\alpha^2\epsilon^2\mu_n^2 \left(a^2 - \frac{b^2}{16}\right)^2. \quad (40)$$

at low momentum transfer. (The normalization can be deduced by considering the limits $a = 0, b \rightarrow \infty$ or *vice versa* where the usual Feynman rules for the amplitude with no form factor apply.) The direct detection limits from LUX [36], CRESST-II [37] and CDMSlite [38] through the kinetic mixing portal are shown for various values of R_2 in figure 6, assuming α_g saturates the constraint (51) from ionization of \mathbf{H}_2 atoms that we will derive in the next section. (We also show the constraints for the fixed value of $\alpha_g = 0.01$ as dashed curves.) Unlike with the dark atoms, the form factor never vanishes for any value of R_2 (since b is always $< 4a$).

For the Higgs portal, we follow the procedure in section 3. The amplitude and cross section are

$$\mathcal{M} = \bar{u}_{\mathbf{H}_2}(p_3)u_{\mathbf{H}_2}(p_1) \cdot \bar{u}_n(p_4)u_n(p_2) \left(\frac{y_n m_n}{v}\right) \times \left(\frac{c_\theta s_\theta}{m_h^2} - \frac{c_\theta s_\theta}{m_\phi^2}\right) (y_1 F_\psi(q) + g F_B(q)) \quad (41)$$

$$\sigma_n \cong \frac{1}{\pi v^2} [(y_1 F_\psi(0) + g F_B(0)) y_n m_n \mu_n \theta]^2 \times (m_\phi^{-2} - m_h^{-2})^2. \quad (42)$$

We have again made the approximation $\theta \ll 1$ and assumed a small momentum transfer. μ_n is the \mathbf{H}_2 -nucleon reduced mass, and $y_n \cong 0.3$ is the Higgs coupling to nucleons (modulo m_n/v). The form factors are given by

$$F_\psi(q) = \frac{2m_\Psi}{m_{\mathbf{H}_2}} e^{-b^2 q^2/32} \\ F_B(q) = \frac{m_B}{2m_{\mathbf{H}_2}} \frac{1}{(1 + \frac{1}{4}a^2 q^2)^2}. \quad (43)$$

Redefining $\tilde{F} = (y_1 F_\psi(0) + g F_B(0))\theta|1 - m_h^2/m_\phi^2|$, the constraint on \tilde{F} from the LUX, CRESST-II and CDMSlite experiments takes the same form as was previously shown in figure 2 (right), where $m_{\mathbf{H}}$ is reinterpreted as $m_{\mathbf{H}_2}$.

4.3. Neutron Star Constraints

Tight constraints exist on the cross section for asymmetric bosonic dark matter scattering on nucleons from the existence of long-lived neutron stars [42, 43]. If the rate of dark matter accretion is large enough, it can collapse to form a black hole that would consume the progenitor, on time scales shorter than the ages of neutron stars observed in globular clusters. In our model it is important that we have only one kind of stable bosonic dark matter constituent carrying dark $U(1)_h$ charge. In the case of \mathbf{H} atoms with only fermionic constituents, the would-be scalar constituents decayed early in the cosmological history, leaving no asymmetric scalars. For \mathbf{H}_2 atoms, on the other hand, the vector bosons are mostly bound inside of atoms that resist collapse because of the degeneracy pressure of their fermionic constituents. The ionized fraction also resists collapse because of dark Coulomb repulsion. In contrast, in a model containing two species of bosons carrying different $U(1)_h$ charges, nothing would prevent the collapse of the combined bosonic fluid.

In more detail, we first note that the dark atoms remain bound once they start to accumulate in the neutron star. From figure 5, the binding energy is given by

$$E_b \approx 2\alpha_g^2 m_B = \frac{2\alpha_g^2 m_{\mathbf{H}_2}}{1 + 2R_2} \quad (44)$$

Using the dark ionization constraint (51), we find that $E_b > 130$ eV even for the extreme parameter choices $m_{\mathbf{H}_2} = 1$ GeV, $R_2 = 100$, which is higher than the temperature of the star, of order 100 eV [44]. Moreover fermions within a neutron star are supported by their degeneracy pressure, given by

$$p = \frac{(3\pi^2)^{2/3}}{5 m_\psi} n_\psi^{5/3}, \quad (45)$$

where n is the number density. A larger fermion mass decreases the pressure, and therefore the dark atoms will tend to remain bound.

As for any ionized bosons that accumulate within the neutron star, their repulsive self-interaction greatly weakens the bounds on scattering with nucleons by preventing their collapse into a black hole. Ref. [45] finds that a repulsive scattering cross section exceeding 10^{-50} cm² is sufficient to avoid neutron star constraints for $m_B < 1$ TeV. In our case the cross section corresponding to dark Rutherford scattering is infrared divergent, but if we make it finite by multiplying $d\sigma/d\Omega$ by $(1 - \cos\theta)^2$ (thus

taking into account only scatterings with significant momentum transfer), it is of order $\alpha_g^2/m_B^2 \gtrsim 10^{-34} \text{ cm}^2$, where we used (51) and $m_B \lesssim 100 \text{ GeV}$. This satisfies the requirements of [45] by many orders of magnitude.

5. OTHER CONSTRAINTS

Dark atoms, dark matter with millicharges, and models with asymmetric dark bosons are subject to further constraints from cosmological, astrophysical and laboratory probes. Here we discuss those coming from dark recombination, self-interactions of the dark matter and accumulation in neutron stars, and searches for millicharged particles.

5.1. Dark ions

If the constituents of the hidden sector fail to combine into atoms, they can scatter very strongly with each other through the dark Coulomb interaction, contradicting the normally assumed properties of collisionless cold dark matter. From fitting to results of ref. [4], one finds that the ionization fraction can be estimated as [14, 21, 23]

$$X_e \cong \left(1 + 10^{10} f_2(R) \xi^{-1} \alpha_g^4 \frac{\text{GeV}^2}{m_{\mathbf{H}}^2} \right)^{-1} \quad (46)$$

where $f_2(R) = R + 2 + 1/R$ (introduced in eq. (20)), and ξ is the ratio of dark sector to SM sector temperatures.

In [4] it was argued that observations of the Bullet Cluster rule out $X_e \gtrsim 0.1$, leading to the conservative lower limit $\alpha_g > \alpha_{\text{ion}}$ (19) that we already incorporated in our analysis of direct detection constraints. Ref. [14] estimates that there is a factor of 10 uncertainty in (46). We note that this leads to only a factor of 1.8 uncertainty in the expression for α_{ion} .

The ratio between temperatures can be found using the relation [14]

$$\xi = \left(\frac{g_{*S,SM}^0 g_{*S,D}^{\text{dec}}}{g_{*S,SM}^{\text{dec}} g_{*S,D}^0} \right)^{1/3}, \quad (47)$$

with $g_{*S,SM}$ and $g_{*S,D}$ denoting the number of degrees of freedom in the visible and dark sectors, and the superscripts 0, dec indicating the respective values today and at the time the two sectors decouple kinetically. The temperature at which this decoupling occurs is therefore relevant. We find that mixed Compton scattering with one dark and one SM photons is the most important process for maintaining kinetic equilibrium. It goes out of equilibrium when $H = n_\gamma \langle \sigma v \rangle$, leading to the estimate

$$1.66 g_* \frac{T^2}{m_{\text{Pl}}} \sim g_* T^3 \frac{8\pi \epsilon^2 \alpha^2}{3 m_{\mathbf{H}}^2}, \quad (48)$$

Thus mixed Compton scattering keeps the two sectors at the same temperature until

$$T_{\text{dec}} = \frac{3 \times 10^{-6} \text{ eV}}{\epsilon^2} \left(\frac{m_{\mathbf{H}}}{\text{GeV}} \right) \quad (49)$$

The lowest value of T_{dec} is obtained by saturating the direct detection limits on ϵ as a function of $m_{\mathbf{H}}$, as shown in figs. 2-3. In the case of $R = 1$ (equal mass dark atom constituents), this can be much lower than the dark recombination temperature T_{rec} , so that in fact $T_{\text{dec}} = T_{\text{rec}}$, since Compton scattering is no longer efficient on neutral atoms. For $R > 1$ on the other hand, the constraints on ϵ are sufficiently strong that the decoupling temperature is limited to $T_{\text{dec}} > 300 \text{ TeV}$.

As long as $T_{\text{dec}} \gg 1 \text{ TeV}$, all particles are relativistic except for the heavy neutrinos. We therefore use the values $g_{*S,SM}^0 = 3.94$ [15], $g_{*S,SM}^{\text{Dec}} = 106.75$, $g_{*S,D}^0 = 2$, and $g_{*S,D}^{\text{Dec}} = 18$. The resulting temperature ratio is $\xi \approx 0.71$. At the other extreme, decoupling occurs after electrons have frozen out. This corresponds to $g_{*S,SM}^{\text{Dec}} = 7.25$, $g_{*S,D}^{\text{Dec}} = 2$, and $\xi \approx 0.81$. Even at the two extremes, therefore, the difference is minimal, and is further mitigated by the fact that ξ is raised to the $1/4$ power in calculating α_{ion} . We therefore adopt the value $\xi = 0.71$ in eq. (19) so that α_{ion} remains a reasonable lower limit for α_g .

There are certain cases that can lead to a lower temperature ratio, with the smallest being that in which all dark content apart from the dark photon has frozen out prior to the freeze-out of the top quark, with decoupling occurring some time between these; in this case the dark temperature could be as low as 0.3. These cases, however, are unrepresentative and only apply to a narrow range of values of ϵ . Even in the extreme case of $\xi \approx 0.3$, the estimate on α_{ion} would only differ by a factor of ≈ 0.8 , which is smaller than the error due to the uncertainty in the ionization fraction.

5.1.1. \mathbf{H}_2 ionization

For the case where Ψ_2 can decay to Ψ_1 and the vector boson B , to make a rough estimate of the ionization fraction, we assume that recombination will typically happen in two steps: in the first, unbound Ψ_1 's combine with the free B 's to make a Ψ - B ion, while in the second these ions bind with a second Ψ_1 . The first step is similar to hydrogen atom recombination with the substitution $\alpha_g \rightarrow 2\alpha_g$ due to B having charge 2. In the second step, the potential at long range is like that for hydrogen atom recombination. Equation (46) then becomes

$$\begin{aligned} X_{e1} &\cong \left(1 + \xi^{-1} 16 \times 10^{10} \alpha_g^4 \frac{\text{GeV}}{m_1 m_B} \right)^{-1} \\ X_{e2} &\cong \left(1 + \xi^{-1} 10^{10} \alpha_g^4 \frac{\text{GeV}}{m_1 (m_B + m_1)} \right)^{-1} \\ X_{e,\text{tot}} &= X_{e1} + X_{e2} \cong X_{e2} \end{aligned} \quad (50)$$

The constraint on the ionization fraction ($X_{e,\text{tot}} \lesssim 0.1$) from [4] is therefore

$$\alpha_g \gtrsim \xi^{1/4} 4 \times 10^{-3} \left(\frac{m_{\mathbf{H}_2}}{\text{GeV}} \right)^{1/2} f_3^{-1/4}(R_2) \quad (51)$$

where $f_3(R_2) = (R_2 + 1/2)^2 / (R_2 + R_2^2)$.

5.2. Self interactions

Although standard cold dark matter is considered to be noninteracting with itself, there has been interest in variant theories where dark matter has an elastic self-scattering cross section of order 1b per GeV of DM mass. This has been motivated by persistent discrepancies between predictions of N -body simulations and observed properties of dark matter halos. While simulations tend to predict cuspy density profiles for galaxies, there is some observational evidence for cored profiles, especially in dwarf spheroidals. Simulations also tend to predict too many high-mass satellite galaxies accompanying Milky-Way like progenitors compared to observations. For a review of these problems and their possible resolutions, see ref. [46]. A number of studies have been done indicating that the small-scale structure problems can be alleviated by invoking dark matter elastic scattering with $\sigma/m \sim 1\text{b/GeV}$. Dark atoms can naturally accommodate such large cross sections since they can have a significant geometric size.

The elastic scattering of dark atoms on each other has been studied very quantitatively, thanks to the fact that the problem can be mapped onto that of normal atom scattering with appropriate rescalings of parameters [16]. A useful rough estimate is that the scattering cross section goes as $\sigma \cong 100 a_0^2 \cong 100 \alpha_g^{-2} f_2^2(R) m_{\mathbf{H}}^{-2}$. A cosmologically interesting level of self-scattering requires $\sigma/m_{\mathbf{H}} \sim 1.1\text{b/GeV} \cong 2800\text{GeV}^{-3}$ [47] in order to address the structure formation problems of cold dark matter. This corresponds to a gauge coupling of

$$\alpha_g = 0.2 f_2(R) (m_{\mathbf{H}}/\text{GeV})^{-3/2} \quad (52)$$

The criterion (52) can be compatible with the ionization constraint (19) if $m_{\mathbf{H}}$ is sufficiently small,

$$m_{\mathbf{H}} \lesssim 14\text{ GeV} \left(\frac{f(R)}{4} \right)^{5/8} \quad (53)$$

obtained from eliminating α_g from the two relations. Very large values of R would be unnatural in our model, since it would require a fine-tuned cancellation between two contributions to $m_1^2 = (m_\psi - y_1\sigma)^2 + (y_2\sigma)^2$, as well as a small value of y_2 . An accidental cancellation at the level of $R = 10$ would allow for $m_{\mathbf{H}}$ as large as 28 GeV.

5.2.1. \mathbf{H}_2 self-interactions

In the \mathbf{H}_2 phase of the theory, the size of the atom is determined by the length scale a that describes the vector

boson part of the wave function, rather than the characteristic distance b between the fermions, even though $b \sim 2a$. This is because the expectation values are $\langle r \rangle = 1.5a$, $\langle \Delta/s \rangle = 0.4b$. Therefore in parallel to the \mathbf{H} atom case, we can estimate the elastic cross section for atom-atom scattering as $\sigma \cong 100 a^2 \cong 100 \alpha_g^{-2} m_{\mathbf{H}_2}^{-2} R_2^2 f_4^2(R_2)$, where $f_4(R) = 1 + (2R_2)^{-1}$.

The gauge coupling corresponding to the desired scattering cross section of $\sigma/m_{\mathbf{H}_2} = 1.1\text{b/GeV}$ is therefore

$$\alpha_g = 0.19 R_2 f_4(R_2) \left(\frac{m_{\mathbf{H}_2}}{\text{GeV}} \right)^{-3/2}. \quad (54)$$

When combined with the constraint (51) on the ionization fraction, the result is

$$m_{\mathbf{H}_2} \lesssim 6.9\text{ GeV} R_2 f_4 f_3^{-1/4}, \quad (55)$$

which is similar to the expression found for the \mathbf{H} case. The primary difference here is that large values of R_2 can be obtained without fine-tuning of model parameters, allowing for a larger natural range of masses consistent with both the ionization fraction and self-interaction constraints. (Notice that $f_{3,4} \rightarrow 1$ as R_2 becomes large.) Even with a moderate hierarchy $R_2 = 10$, we can reach masses as large as $m_{\mathbf{H}_2} \sim 70\text{ GeV}$.

5.3. Laboratory millicharge searches

Pair production of $\bar{\Psi}_i \Psi_i$ is possible in accelerator experiments from the coupling of the photon to the dark matter millicharge. The resulting constraints on ϵ are quite weak in the mass range relevant for our model, $m_{\mathbf{H}} \sim 1 - 100\text{ GeV}$, as we show in fig. 7. The existing constraints are taken from tables in ref. [48] for the ASP and trident production limits, the E613 beam dump limit [49], ALEPH limits on the Z decay width [50] and a recent CMS search for particles of charge 1/3 or 2/3 [51]. We also show the reach of a new proposed experiment for LHC (dashed curve) [52]. These constraints are considerably weaker than that coming from direct detection, fig. (3), which is replotted as the dashed curve on fig. 7. Only at low ($m_{\mathbf{H}} \lesssim 4\text{ GeV}$) or high ($m_{\mathbf{H}} < 100\text{ GeV}$) masses, outside the sensitivity of direct detection, do they become dominant.

Possibly more significant constraints on millicharged particles arise from searches for exotic isotopes, bound states of normal nuclei with the charged DM constituents. Very stringent limits on the concentration of heavy isotopes of hydrogen or oxygen from sea water have been derived; for example ref. [53]) obtains an upper bound of 10^{-28} for the concentration of anomalously heavy H. These experiments assume integer-charged ions, but a recent experiment geared toward millicharged particles with $\epsilon > 10^{-5}$ set a limit of 10^{-14} on the abundance per nucleon. Naively such results would seem to rule out almost any values of $\epsilon \gtrsim 10^{-3}$ such that the binding energy $E_b \cong \frac{1}{2}(\alpha\epsilon)^2 m_p$ (for anomalous H) exceeds kT at room

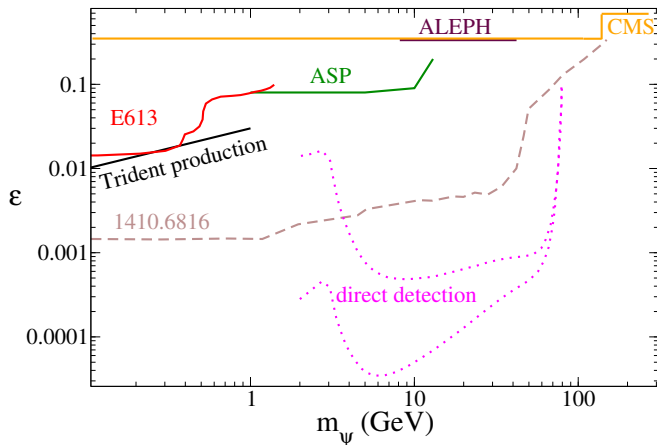


FIG. 7: Solid curves: existing collider constraints on millicharge versus mass; dashed curve: expected reach of experiment proposed in ref. [52]. Dotted curves: our direct detection limits from fig. 3, depending on choice of $\alpha_g = 0.06$ (upper curve) or $\alpha_g = \alpha_{\text{ion}}$ (lower).

temperature, since we expect some fraction of ψ particles to remain ionized and thus be able to contaminate normal matter.

However to translate these limits on abundances into bounds on ϵ requires many considerations, including the expected flux of ψ particles, their capture cross section on the elements in question, the shielding of the earth and the galaxy from charged particles by magnetic fields, expulsion of charged particles by supernova winds, the process of purification of the samples studied, and the question of whether they apply to noninteger charged isotopes [21]. A recent study of these issues was presented in ref. [54]. Here we take the view that there may be room for evading the anomalous isotope searches, but this question should be revisited if positive evidence for millicharges is found.

6. CONCLUSION

In this work we have tried to strike a balance between simplicity and realism in the construction of an atomic dark matter model. Our nonabelian construction is sufficiently rich to explain a unified origin of the massless dark photon and charged (under the hidden $U(1)_h$ interaction) DM constituents Ψ_i as a consequence of symmetry breaking $SU(2)_h \rightarrow U(1)_h$ by a scalar triplet VEV in the dark sector. With the addition of a dark Higgs doublet, we have the necessary ingredients to explain the Ψ_i asymmetry through leptogenesis, simultaneously with the baryon asymmetry. Electric millicharges of Ψ_i , while not a necessary ingredient, can arise naturally through

heavy states carrying both electric and $U(1)_h$ charge. Higgs portal interactions are also optional, but are allowed by a dimension-4 interaction of Ψ_i with the dark Higgs triplet and its mixing with the SM Higgs.

The model is mainly testable by direct detection. For sufficiently light or heavy constituents, the DM could also be discovered in an experiment proposed for LHC to probe millicharged particles. It can accommodate strong DM self-interactions as suggested by problems of Λ CDM simulations to correctly predict the small-scale structure of galaxies, if the dark atoms are not too heavy. Because of the requirement $\alpha_g \gtrsim \alpha_{\text{ion}}$, needed to make the ionization fraction in the dark sector sufficiently small, the symmetric component of the dark matter is highly suppressed due to annihilations into dark photons, making any indirect signals too weak to be detected.

Our model has a number of features that distinguish it from simplified atomic dark matter models. For example in the latter, the ratio R of the masses of the atomic constituents (which plays an important role) can be arbitrarily large, whereas here it is naturally of order 1, and requires fine-tuning to be much greater.

If the new Yukawa coupling y_1 exceeds the gauge coupling g , the stable dark matter particles can be the lighter fermion Ψ_1 and the doubly charged (under $U(1)_h$) vector boson B^{--} , leading to novel three-body $B\Psi\Psi$ bound states, where the mass ratio of the constituents m_1/m_B could be large without tuning of parameters (other than the usual hierarchy problem of light bosons). The properties of these unusual atoms for direct detection, as well as for DM self-interactions, are qualitatively similar to those of the more conventional two-constituent atoms. This demonstrates a loophole for strong neutron star constraints on asymmetric bosonic dark matter, since the dark Coulomb repulsion prevents Bose condensation in this model.

For future work, these models suggest a potential novel signal for direct detection, due to the possible simultaneous presence of both dark atoms and a subdominant component of ionized or symmetric constituents. This would allow for the detection of both types of dark matter, typically having similar but distinct masses and interaction cross sections. Our analysis of leptogenesis as a common origin of the visible and hidden asymmetries is approximate, and it might also be interesting to undertake a more refined treatment for future studies.

Acknowledgments. We thank Sacha Davidson, Kimmo Kainulainen, Tim Linden, Zuwei Liu, Wei Xue and Wells Wulsin for helpful correspondence or discussion. We acknowledge support of the Natural Sciences and Engineering Research Council of Canada. We are grateful to NBIA for its generous hospitality while we were completing this work.

[1] M. Pospelov, A. Ritz, and M. B. Voloshin, *Phys.Lett. B* **662**, 53 (2008), 0711.4866.

[2] N. Arkani-Hamed, D. P. Finkbeiner, T. R. Slatyer, and

- N. Weiner, Phys.Rev. **D79**, 015014 (2009), 0810.0713.
- [3] J. L. Feng, M. Kaplinghat, H. Tu, and H.-B. Yu, JCAP **0907**, 004 (2009), 0905.3039.
- [4] D. E. Kaplan, G. Z. Krnjaic, K. R. Rehermann, and C. M. Wells, JCAP **1005**, 021 (2010), 0909.0753.
- [5] D. E. Kaplan, G. Z. Krnjaic, K. R. Rehermann, and C. M. Wells, JCAP **1110**, 011 (2011), 1105.2073.
- [6] J. Fan, A. Katz, L. Randall, and M. Reece, Phys.Rev.Lett. **110**, 211302 (2013), 1303.3271.
- [7] J. Fan, A. Katz, L. Randall, and M. Reece, Phys.Dark Univ. **2**, 139 (2013), 1303.1521.
- [8] R. Foot, Int. J. Mod. Phys. **A29**, 1430013 (2014), 1401.3965.
- [9] I. García García, R. Lasenby, and J. March-Russell, (2015), 1505.07410.
- [10] J. Fan, A. Katz, and J. Shelton, JCAP **1406**, 059 (2014), 1312.1336.
- [11] R. Foot and S. Vagnozzi, Phys. Lett. **B748**, 61 (2015), 1412.0762.
- [12] M. T. Frandsen, F. Sannino, I. M. Shoemaker, and O. Svendsen, JCAP **1405**, 033 (2014), 1403.1570.
- [13] L. Pearce, K. Petraki, and A. Kusenko, Phys. Rev. **D91**, 083532 (2015), 1502.01755.
- [14] F.-Y. Cyr-Racine and K. Sigurdson, Phys. Rev. **D87**, 103515 (2013), 1209.5752.
- [15] F.-Y. Cyr-Racine, R. de Putter, A. Raccanelli, and K. Sigurdson, Phys. Rev. **D89**, 063517 (2014), 1310.3278.
- [16] J. M. Cline, Z. Liu, G. Moore, and W. Xue, Phys. Rev. **D89**, 043514 (2014), 1311.6468.
- [17] J. M. Cline, Z. Liu, G. Moore, and W. Xue, Phys. Rev. **D90**, 015023 (2014), 1312.3325.
- [18] R. Foot and S. Vagnozzi, Phys. Rev. **D91**, 023512 (2015), 1409.7174.
- [19] K. Petraki, L. Pearce, and A. Kusenko, JCAP **1407**, 039 (2014), 1403.1077.
- [20] B. Holdom, Phys.Lett. **B166**, 196 (1986).
- [21] J. M. Cline, Z. Liu, and W. Xue, Phys.Rev. **D85**, 101302 (2012), 1201.4858.
- [22] J. M. Cline, Z. Liu, and W. Xue, Phys. Rev. **D87**, 015001 (2013), 1207.3039.
- [23] J. M. Cline, Y. Farzan, Z. Liu, G. D. Moore, and W. Xue, Phys. Rev. **D89**, 121302 (2014), 1404.3729.
- [24] L. Ackerman, M. R. Buckley, S. M. Carroll, and M. Kamionkowski, Phys. Rev. **D79**, 023519 (2009), 0810.5126, [277(2008)].
- [25] H. An, S.-L. Chen, R. N. Mohapatra, and Y. Zhang, JHEP **03**, 124 (2010), 0911.4463.
- [26] E. J. Chun, Phys. Rev. **D83**, 053004 (2011), 1009.0983.
- [27] E. J. Chun, JHEP **03**, 098 (2011), 1102.3455.
- [28] C. Arina and N. Sahu, Nucl. Phys. **B854**, 666 (2012), 1108.3967.
- [29] A. Falkowski, J. T. Ruderman, and T. Volansky, JHEP **1105**, 106 (2011), 1101.4936.
- [30] W.-Z. Feng and P. Nath, Phys. Lett. **B731**, 43 (2014), 1312.1334.
- [31] F. Chen, J. M. Cline, and A. R. Frey, Phys.Rev. **D80**, 083516 (2009), 0907.4746.
- [32] E. Witten, Phys.Lett. **B117**, 324 (1982).
- [33] W. Buchmuller, P. Di Bari, and M. Plumacher, Annals Phys. **315**, 305 (2005), hep-ph/0401240.
- [34] S. Davidson and A. Ibarra, Phys. Lett. **B535**, 25 (2002), hep-ph/0202239.
- [35] T. R. Slatyer, Phys. Rev. **D87**, 123513 (2013), 1211.0283.
- [36] LUX Collaboration, D. Akerib *et al.*, Phys.Rev.Lett. **112**, 091303 (2014), 1310.8214.
- [37] CRESST, G. Angloher *et al.*, (2015), 1509.01515.
- [38] SuperCDMS, R. Agnese *et al.*, Submitted to: Phys. Rev. Lett. (2015), 1509.02448.
- [39] SuperCDMS, R. Agnese *et al.*, Phys. Rev. Lett. **112**, 241302 (2014), 1402.7137.
- [40] J. M. Cline, K. Kainulainen, P. Scott, and C. Weniger, Phys.Rev. **D88**, 055025 (2013), 1306.4710.
- [41] DELPHI, OPAL, ALEPH, LEP Working Group for Higgs Boson Searches, L3, S. Schael *et al.*, Eur. Phys. J. **C47**, 547 (2006), hep-ex/0602042.
- [42] I. Goldman and S. Nussinov, Phys. Rev. **D40**, 3221 (1989).
- [43] S. D. McDermott, H.-B. Yu, and K. M. Zurek, Phys. Rev. **D85**, 023519 (2012), 1103.5472.
- [44] K. M. Zurek, Phys.Rept. **537**, 91 (2014), 1308.0338.
- [45] C. Kouvaris and P. Tinyakov, Phys. Rev. Lett. **107**, 091301 (2011), 1104.0382.
- [46] D. H. Weinberg, J. S. Bullock, F. Governato, R. K. de Naray, and A. H. G. Peter, (2013), 1306.0913.
- [47] J. Zavala, M. Vogelsberger, and M. G. Walker, Monthly Notices of the Royal Astronomical Society: Letters **431**, L20 (2013), 1211.6426.
- [48] S. Davidson, B. Campbell, and D. Bailey, Phys. Rev. D **43**, 2314 (1991).
- [49] E. Golowich and R. W. Robinett, Phys. Rev. D **35**, 391 (1987).
- [50] ALEPH, D. Buskulic *et al.*, Phys. Lett. **B303**, 198 (1993).
- [51] CMS, S. Chatrchyan *et al.*, Phys. Rev. **D87**, 092008 (2013), 1210.2311.
- [52] A. Haas, C. S. Hill, E. Izaguirre, and I. Yavin, Phys. Lett. **B746**, 117 (2015), 1410.6816.
- [53] P. F. Smith *et al.*, Nucl. Phys. **B206**, 333 (1982).
- [54] C. Kouvaris, Phys. Rev. **D88**, 015001 (2013), 1304.7476.
- [55] A. Geringer-Sameth *et al.*, (2015), 1503.02320.
- [56] M. L. Graesser, I. M. Shoemaker, and L. Vecchi, JHEP **10**, 110 (2011), 1103.2771.
- [57] J. M. Cline and P. Scott, JCAP **1303**, 044 (2013), 1301.5908.
- [58] M. Ackermann *et al.*, Phys. Rev. **D91**, 122002 (2015).
- [59] M. Abdullah *et al.*, Phys. Rev. **D90**, 035004 (2014), 1404.6528.
- [60] J. M. Cline, G. Dupuis, Z. Liu, and W. Xue, Phys. Rev. **D91**, 115010 (2015), 1503.08213.
- [61] Fermi-LAT, M. Ackermann *et al.*, (2015), 1503.02641.
- [62] DES, Fermi-LAT, A. Drlica-Wagner *et al.*, Submitted to: Astrophys. J. (2015), 1503.02632.
- [63] D. Hooper and T. Linden, (2015), 1503.06209.
- [64] V. Bonnivard *et al.*, (2015), 1504.03309.